ATS MATERIALS/MANUFACTURING*

M. A. Karnitz (karnitzma@ornl.gov;423-574-5150)
I. G. Wright (wrightig@ornl.gov;423-574-4451)
M. K. Ferber (ferbermk@ornl.gov;423-576-0818)
R. S. Holcomb (holcomb@ornl.gov; 423-574-0273)
Oak Ridge National Laboratory
P. O. Box 2008
Oak Ridge, TN 37831-6065

Mary H. Rawlins (rawlinsmh@ornl.gov;423-576-4507)
U. S. Department of Energy-Oak Ridge
P. O. Box 2008
Oak Ridge, TN 378316-6269

ABSTRACT

The Materials/Manufacturing Technology subelement is a part of the base technology portion of the Advanced Turbine Systems (ATS) Program. The work in this subelement is being performed predominantly by industry with assistance from national laboratories and universities. The projects in this subelement are aimed toward hastening the incorporation of new materials and components in gas turbines. Work is currently ongoing on thermal barrier coatings (TBCs), the scale-up of single crystal airfoil manufacturing technologies, materials characterization, and technology information exchange. This paper presents highlights of the activities during the past year.

OBJECTIVES

The primary objective of the materials/manufacturing element is to provide materials and material-related manufacturing technology support to the ATS projects and to the gas turbine industry at large. The ATS prime contractors are responsible for the technologies necessary for the demonstration projects. The materials/manufacturing support is intended to complement the ATS team efforts and provide expertise not available to any single contractor.

INTRODUCTION

The original ATS Materials/ Manufacturing Plan was developed in April 1994,[1] and focuses on generic materials issues, components, and manufacturing processes. The plan was developed in coordination with the turbine manufacturers and there has been a continuing interaction with manufacturers since the publication of the plan. The manufacturers have stated a need for turbine inlet temperatures as high as 2600 F to achieve the ATS efficiency goals. To achieve these temperatures for extended operating periods, there is a need to utilize new materials. Manufacturers also indicated a need for effective interaction among themselves, materials suppliers, universities, national laboratories, and others.

A new Materials/Manufacturing Needs Statement was issued in December 1996. The new needs statement reiterated some of the major concerns brought forth in the original plan, however, more detail was provided in several major categories. The new needs statement summarizes continuing needs on (1) coating process development, (2) single-crystal airfoil manufacturing technology, (3) turbine airfoil development, and (4) ceramic development. The plan also identifies additional needs on (1) long-term

*Research sponsored by U. S. Department of Energy's Office of Energy's Office of Energy Efficiency and Renewable Energy (Office of Industrial Technologies and Office of Fossil Energy (Morgantown Energy Technology Center) for the Advanced Turbine Systems Program, under contract DE-AC05-96OR22464 with Lockheed Martin Energy Research Corporation.

high-temperature data for life prediction and reliability, (2) advanced cooling concepts, (3) abradable turbine blade seals, (4) disc alloy development for long-term creep strength, and (5) maintenance, repairs, and inspection.

PROJECT DESCRIPTION

The Materials/Manufacturing subelement has projects underway in four major categories. There are now projects ongoing in coatings and process development, scale-up of single crystal airfoil manufacturing, materials characterization, and technology information exchange. This section of the paper summarizes the ongoing activities in these four categories.

The focus of the coating and process development projects is to provide TBC systems for land-based gas turbines. The TBC/bond coat system projects are the highest priority within the materials/manufacturing element. Two projects are underway in this area;, one with Westinghouse Power Generation Business Unit in Orlando, Florida and another with Pratt & Whitney of East Hartford, Connecticut. Both projects were initiated in August 1995. The goal of these programs is the development of dependable TBCs that enable increased turbine inlet temperatures while maintaining airfoil substrate temperatures at levels to meet the ATS goals. These are multiphase projects for which Phase I is TBC process development, Phase II is bench testing, and Phase III is product line gas turbine testing. The contractors are currently working on both Phase I and Phase II. Complete descriptions and highlights of these projects are addressed separately in papers in this proceedings by Westinghouse and Pratt & Whitney.

Projects are also underway to develop the capability of single-crystal airfoils for land-based turbines. There are currently two projects, one with Howmet Corporation in Whitehall, Michigan and another with PCC Airfoils in Cleveland, Ohio. The project led by Howmet is supported by a team including ABB, Pratt & Whitney, Solar Turbines, and Westinghouse. The project includes four main thrust areas:

*Low sulfur alloys
*Casting process development
*Post-casting process development
*Casting defect tolerance levels

This project was initiated in May 1995 and will be completed at the end of 1998. A detailed description of the project and the highlights are presented in a separate paper in these proceedings by Howmet.

The PCC Airfoils Project is supported by General Electric Power Generation and has four major tasks:

*Alloy melt practice
*Modification/improvement of single-crystal casting processes
*Core material and design
*Grain orientation control

The PCC Airfoils Project was initiated in March 1995 and will also be completed at the end of 1998. The project is described in more detail in a separate paper in these proceedings by PCC Airfoils.

There are two main projects under the materials characterization category. One is on long-term testing of ceramics and ceramic matrix composites for gas turbines, the other on TBC characterization. The Department of Energy's Office of Industrial Technologies initiated a program in 1992 to develop ceramic components for use in industrial gas turbines. The program was designed to bring ceramic technologies to the point where short-term reliability and engine performance can be demonstrated. Solar Turbines, Inc. was selected for the development of the ceramic gas turbine components. One of the critical areas outlined in this program was a long-term materials testing program. Long-term materials testing is needed to determine the survivability of the materials for land-based applications.

As a subset of the Solar Turbines program, ORNL and the University of Dayton Research Institute (UDRI) initiated research activities that focused on the evaluation of the static tensile creep and stress rupture behavior of several commercially available structural

ceramics. These materials were identified by the gas turbine manufacturers as leading candidates for use in industrial gas turbines. Because the available information for many candidate structural ceramics was limited to less than 2,000 hours, this project was focused on extending these data to times on the order of 10,000 hours. This time period represents the lower limit of operating time anticipated for ceramic blades and vanes in industrial gas turbine engines.

The TBC Characterization Projects are focused on the development of characterization techniques for the evaluation of the mechanical and thermal reliability of TBCs. An extensive review of the characterization techniques helped focus the program on several of the most promising techniques for further evaluation. Emphasis is being placed upon methods for appropriately measuring residual stress, thermal conductivity, and damage in the form of micro and macro cracking and oxidation.

The information exchange category of the Materials/Manufacturing Element has mainly focused on proving a mechanism for transfer of information on the materials issues developed by other agencies such as NASA, DOD, and other DOE materials programs to the ATS Program. Some of these materials efforts have significant impact on the ATS Program. One example of this is a jointly sponsored TBC workshop that was held in conjunction with NASA and NIST in Cincinnati, Ohio on May 13-14, 1997. This was the second workshop that was jointly sponsored among three agencies. The objective of this workshop, and the earlier one, was to assess the state of TBC knowledge and identify critical gaps in knowledge that hinder their use in advanced applications.

ACCOMPLISHMENTS

As mentioned previously, the results for the coatings and process development projects and the scale-up of single-crystal airfoil projects are described in separate papers in these proceedings and are, therefore, not covered in this paper. The results presented in this paper will focus on the materials characterization subelement for both the long-term testing of ceramics and the TBC characterization.

Long Term Testing

Structural ceramics such as silicon carbide and silicon nitride are currently candidates for application as high-temperature components in land-based industrial gas turbines.[2-4] Metallic components which have been targeted for replacement by these ceramic materials include vanes, blades, shrouds, and combustor liners. The use of ceramics over metallic materials has been stimulated by the potential for higher operating temperatures and thus, higher engine efficiencies. However, because industrial turbines are expected to operate continuously for periods of 30,000+ hours between overhauls, the long-term mechanical reliability of the ceramic components is a major concern. Time-dependent processes such as creep, slow crack growth, oxidation , and cyclic fatigue can result in a continuous reduction in the component strength. Premature failure of the component can occur if the strength drops below the maximum service stress.

Efforts to predict the lifetime of ceramic components have been limited by two factors. First, much of the available stress (creep) rupture data describing time-dependent failure are limited to times of 2000 hours or less. However, in order to assure confidence in the predicted components' lives, engine designers have stressed the need for data covering at least 10,000 hours. Second, many of the candidate ceramic materials under consideration are relatively new and thus, few data are available.

This section describes results of a long-term testing program which was initiated in 1992 to address these issues. Research activities in this program focus on four areas: (1) the evaluation of the static tensile creep and stress rupture (SR) behavior of structural ceramics and ceramic matrix composites, (2) modeling of the data generated in Item 1, (3) information exchange, and (4) component evaluation. In the case of Item 1, the long-term testing was supplemented by materials characterization including scanning electron microscopy and x-ray diffraction. Each of these research activities are discussed below.

Long-Term Testing and Characterization. Tensile creep data is being generated in air by measuring creep strain as a function of time, applied stress, and temperature. The SR resistance is evaluated by continuing each creep test until the specimen fails. For each material investigated, a minimum of three temperatures and four stresses is used to establish the stress and temperature sensitivities of the creep and SR behavior. The test matrix utilized in this program is intended to extend the test conditions investigated by the engine component manufacturers. In the latter case, these conditions focus primarily upon the evaluation of the creep and SR behavior of two candidate materials at one temperature only. Consequently, the temperatures chosen for this effort bracket that used by the engine component manufacturers. Because existing data for many candidate structural ceramics are limited to testing times less than 2000 h, this program will focus on extending these data to times on the order of 10000 h, which represents the lower limit of operating time anticipated for ceramic blades and vanes in gas turbine engines.

Table 1 summarizes the materials that are being examined in the Long-Term Testing project. They include four structural ceramics and one ceramic matrix composite. The fabrication of the NT164 is through pressure slip casting for the green state and hot isostatic pressing (HIPing) for the final densification. The microstructure typically consists of β silicon nitride grains having a grain width of less than one micron and an aspect ratio range of 4 to 8. Depending on processing, the α silicon nitride content can range from 5 to 40%.

The SA SiC is a sintered silicon carbide which is fabricated in the green-state by injection molding. Small amounts of carbon and boron are added to assist the densification during sintering. Post-sinter HIPing is also used to improve density and reduce defect size. The microstructure of this material typically consists of α silicon carbide grains ranging in size from 2 to 8 μm.

The SN88 silicon nitride is injection molded followed by gas pressure sintering. Sintering aids include Al_2O_3 and Yb_2O_3.

AS800, which is classified as a self-reinforced silicon nitride, has a microstructure similar to that of SN88 and is of interest to both Solar Turbines and Allison Engines.

SiC/DIMOX is a composite manufactured by Dupont-Lanxide consisting of CG (Ceramic Grade) Nicalon fibers in an aluminum oxide matrix. The fiber architecture consists of an 8 harness satin weave having either a 0-90° or +/-45° lay-up. To reduce the detrimental effects of oxidation, a duplex boron nitride-silicon carbide coating is applied to the fibers (prior to the formation of the matrix) using chemical vapor deposition. The aluminum oxide matrix is formed via the directed metal oxidation of aluminum (DIMOX process). The SiC/DIMOX material is currently being considered for use as a gas turbine component by Westinghouse.

Table 2 summarizes the types of tests conducted on the five material systems. The establishment of tensile stress rupture data covering times from 1 to 10,000 hours is a key objective for all five materials. The NT164 tensile specimens are also being used to validate a new test method combining dynamic fatigue and interrupted stress rupture. Normally dynamic fatigue is used to quickly assess a material's susceptibility to time-dependent fracture by measuring strength as a function of stressing rate. Although one may utilize this information to generate a stress rupture curve, the confidence in the predicted stress rupture lives can be low particularly at the lower stresses. By conducting dynamic fatigue measurements following a static stress for a fixed exposure time (interrupted stress rupture), one should be able to increase the confidence in the stress rupture curve generated from the dynamic fatigue data. The experimental phase of this work, which was conducted at the University of Dayton Research Institute, is now complete. The analysis of data is underway and should be finished within the next few months.

Stress rupture testing of the NT164, SN88, SA SiC, SiC/DIMOX materials were completed. Figures 1-3 illustrate stress

rupture data obtained for the SN88, SA SiC, and SiC/DIMOX, respectively. In general the susceptibility to time-dependent failure as reflected by the slope of the stress rupture curves is less for the SA SiC. However, a major problem with this material is that its relatively low Weibull modulus resulted in considerable uncertainty in both the strength and the rupture time. Consequently during stress rupture testing, many specimens which were subjected to stresses slightly below the average fracture strength failed upon loading. In the case of the SN88, time-dependent strength degradation was evident at all temperatures. The associated mechanism was attributed to the formation of creep cavities and their eventual accumulation into a damage zone originating from the specimen surface.[5,6] An example of one such damage zone is shown in the micrograph (left-hand side) in Fig. 4. The surface cracks observed along the gage section (micrograph on right) indicate that damage zone formation occurred throughout the gage volume. While the susceptibility to time-dependent failure is greater for the SN88 than that for the SA SiC, the stress rupture data for the SN88 are generally much more repeatable. Because this behavior leads to a much greater confidence in the prediction of component lifetime, SN88 is considered to be a better candidate for component fabrication.

As shown in Fig. 3, a significant susceptibility to stress rupture was found for the SiC/DIMOX at both 800 and 1200°C. Based upon related work on SiC/SiC composites,[7] the behavior at the lower temperature may be attributed to the embrittlement of the Nicalon™ fiber which occurs as the protective coating is altered by oxidization. At the higher temperature of 1200°C, creep of the matrix may also play a role in the time-dependent failure process. Because of these problems, this material will no longer be considered as a candidate gas turbine material.

Testing of the AS800 silicon nitride was also continued. As shown in Fig. 5, stress rupture data obtained for this material indicated that the tensile specimens fabricated from the more recent billets were more susceptible to creep rupture. Specimens fabricated from Billets S96063, S96066, S96067, S96069, and S96072 (mid-1996 vintage) had much shorter lifetimes (and much higher creep rates-Fig. 6) than did specimens machined from either Billet S95188 or S96080 (late 1995/early 1996 vintage). Preliminary x-ray data indicated that the billets having the poorer creep resistance contained minor amounts of $Y_8Si_4N_4O_{14}$ (J Phase) while the H-phase was the major phase in the billets with the better creep resistance . A comparison of these latter billets with the SN88 silicon nitride (Fig. 7) revealed comparable stress rupture characteristics.

Modeling. A number of models has been used to describe the stress and temperature sensitivities of creep and creep rupture. The analysis of creep data is typically based upon the assumption that the steady-state or minimum creep strain rate , $d\varepsilon_s/dt$, dominates the overall behavior. For this case, the stress and temperature dependencies of $d\varepsilon_s/dt$ are given by the expression,

$$d\varepsilon_s/dt = A_o (\sigma_a/\sigma'_o)^n \exp(-Q_c/RT), \quad (1)$$

where A_o is a pre-exponential factor, σ_a is the applied stress, σ'_o is a normalizing parameter (i.e. σ'_o=1 MPa), n is the creep (or stress) exponent, Q_c is the activation energy, R is the universal gas constant, and T is the absolute temperature. The fatigue life, t_f, can be described by a similar equation,

$$t_f = B_o (\sigma_a/\sigma'_o)^{-N} \exp(Q_f/RT), \quad (2)$$

where N, Q_f, and B_o now determine the stress and temperature dependencies of the dominant fatigue mechanism. When failure is controlled by the accumulation of creep damage, t_f is often found to be unique function of $d\varepsilon_s/dt$ independent of applied stress and temperature. The relationship between t_f and $d\varepsilon_s/dt$ can be derived by combining Eqs. 1 and 2,

$$t_f = B_o (1/A_o)^{-m} (d\varepsilon_s/dt)^{-m} \exp[(Q_f - mQ_c)/RT], \quad (3)$$

where m = N/n. For the case where $m \approx 1$ and $Q_f \approx Q_c$, one obtains the Monkman-Grant relation,

$$t_f = C_o (d\varepsilon_s/dt)^{-m} \quad (4)$$

where C_o is a constant.

A major problem with the Monkman-Grant relation is that it fails to adequately describe the data over a broad temperature range. This occurs because the power-law stress exponents, n and N, change with temperature. This is illustrated for the SN88 data in Fig. 8 which shows an increase in the absolute magnitude of N with decreasing temperature. A much better description of the experimental data was obtained using the exponential expression,

$$t_f = B \exp(b\sigma) \exp(Q_f/RT), \quad (5)$$

where the parameter b characterizes the exponential stress dependency. The exponential form of Eq. 5 arises if one assumes that the creep process (cavitation), which is responsible for time-dependent failure, is controlled by stress-directed diffusion. As shown by the lines in Fig. 1, the fit of this expression to the experimental data is quite good. Note that the data generated at 1038°C were not included in the analysis because most of the specimens were still under test.

Information Exchange. In order to maintain the relevance of this program to the gas turbine manufacturers involved in the utilization of ceramic components, yearly workshops are held in which current results are presented and future directions are discussed. The most recent workshop was held at UDRI on April 18, 1996 and included representatives from Allison Engines, Solar Turbines, Westinghouse, NIST, ORNL, EPRI, and DOE. Based upon the results of that workshop, several new material systems were added to the long-term test matrix.

Component Characterization. The extensive engine testing at Solar Turbines has resulted in the availability of a number of ceramic components for direct post-test evaluation. To date most of the emphasis has been placed upon elucidating any mechanical and phase changes occurring in AS800 blades subjected to a 100 h engine test. Two as-received and three post-test blades were examined. Figure 9 provides a macroscopic view of a typical post-test blade. As shown in the inset, small white spots were observed on the airfoils of all post-test blades. However subsequent scanning electron microscopy (SEM) of these white spots indicated that their microstructure and elemental composition were identical to unspotted regions.

SEM was used to examine both the surfaces and polished cross sections of the AS800 blades. A cross section for an as-received blade is shown in Fig. 10. The microstructure consisted of elongated grains surrounded by a Y-Si-O-N intergranular phase (light regions in Fig. 10). The surface of the as-received blade was also relatively smooth. In the case of the post-test blades, several interesting features were observed. One of the blades (Fig. 11a) contained a few large crack-like defects located at the surface. The second blade (Fig. 11b) was characterized by a fairly rough surface. While these features were absent in the last blade (Fig. 11c), a near surface region of increased intergranular phase content was found. Energy dispersive x-ray analysis indicated that the yttrium content was lower in this area. The cause of these features is currently under investigation.

Both the as-received and 100 h post-test blades were sectioned into small flexure specimens as shown in Fig. 12. The tensile surfaces of these flexure specimens were not machined so that the strength would directly reflect the surface condition. Preliminary results, Fig. 13, indicate that the 100 h engine test did not reduce the strength of the AS800 air foils.

TBC Characterization

The overall goal of this task is to develop and apply advanced techniques to the characterization of TBCs used in land-base gas turbines. The choice of specific characterization methods was based upon (1) a formal needs assessment conducted as part of the Materials/Manufacturing Program, (2) input from recognized experts, and (3) results from workshops and other meetings

(NASA/DOE/NIST TBC Workshop, ATS Materials Workshop (SCERDC), ATS Review Meeting, IGTI Turbo/Expo, etc.). The following efforts have been initiated since FY95:

Residual Stress
Thermal Gradient Testing
Failure Mechanisms
Thermophysical Properties and Thermal NDE
Oxidation Resistance.

Progress in each of these areas is discussed below.

Residual Stress. The primary goal of this research is to characterize the residual stress state and phases in thermal barrier coatings (TBCs), bond coats, interfaces, and substrates at room and elevated temperatures and under applied load. Research activities will apply diffraction techniques to characterize the residual stresses in research grade and industrial specimens. Knowledge of stress and phase gradients is critical for understanding TBC failure which is typically due to a thermally-grown oxide scale. The room temperature phases, texture, and residual stresses of the thermally-grown scales within and on the three and two layer specimens (i.e., top coat/bond coat/substrate and bond coat/substrate) will be determined as a function of time and temperature (ambient and in-situ) and depth. The microstructures of the TBC, bond coat, and substrate in the as-received and heat treated states will be observed using the SEM. Surface roughness and surface area will be measured by profilometry and BET. This information will be critical for understanding the location and kinetics of oxide scale formation at the interface and sintering behaviors of TBC.

Two EB-PVD YSZ top coat/"PtAl" bond coat/René N5 specimens were examined with an electron microprobe in as-received and heat treated (200 h at 1150 °C ambient) conditions in order to confirm that the layer-like feature in-between the top coat and bond coat was an Al_2O_3-rich layer rather than a crack. In Figure 14a, the thickness of this layer at the top coat/bond coat interface is shown to be 4 μm in the heat treated specimen. Figures 14b and c show the results of energy and wavelength dispersive spectroscopy, respectively, indicating that the dark feature resembling a crack in Figure 14a is actually a layer of predominantly Al_2O_3, which was also identified via x-ray diffraction in a sample which had undergone layer removal. Although not shown, this alumina layer is also present in the as-received sample due to preoxidation, which occurred prior to ZrO_2 deposition.

A thermally grown oxide scale on a "PtAl" bond coat/René N5 sample was examined in-situ using high temperature x-ray diffraction and synchrotron radiation (λ=1.3808 Å). The bond coat and substrate were 0.05 and 0.95 mm thick, respectively. Here, the bare bond coat sample was mounted on a Pt heating strip in a commercially available high temperature furnace for x-ray diffraction. The sample was then heated to 1150 °C. After 48 hours, a scale grew which was ~2 μm thick and predominately alumina. Strain measurements were then made using 2θ scans with a fixed angle of x-ray incidence (asymmetric diffraction). The data was analyzed following the analysis of Sarioglu et al.[8]

Table 3 lists the phases present in the sample before and after heat treatment. After 48 h at 1150 °C, the thin scale did not provide diffraction peaks in the desired high 2θ region (>130 °) for x-ray strain measurement. Thus, lower 2θ peaks were used which inherently provide less sensitivity to strain. Any sample displacement error had a negligible effect on the data due to the parallel nature of the x-ray beam. The measured stress at 1150 °C and at 600 °C were found to be extremely large (> 4 GPa) and suggested some problem with the experiment. These values did show a twofold increase in the stress as the temperature was roughly halved. Due to time constraints, a scan at room temperature was not done at the synchrotron. Three weeks later, a scan was run at ORNL at room temperature. The stress was found to be -3 GPa using 2θ scan with a fixed angle of x-ray incidence. $Sin^2\psi$ measurements were also made on the (116) and (300) reflections using Cu $K\alpha_1$ radiation (λ= 1.5406 Å) which yielded stresses of -1.8 and -1.7 GPa, respectively. The room temperature stress values are similar in

magnitude to those reported elsewhere. Additional $\sin^2\psi$ measurements made at 90° to the aforementioned results yielded the same stress values indicating an isotropic in-plane stress state. Presently, the high temperature results are regarded as preliminary. These experiments were found to be quite challenging, especially sample mounting, and will be repeated in the future.

Thermal Gradient Test System. The useful lifetime of current thermal barrier coating (TBC) systems is generally limited by failure along the TBC/bond coating interface. Failure is driven by a combination of thermal-mechanical cycling and deleterious environmental attack by hot gas constituents. An efficient test method is needed to aid in the development and characterization of TBCs under realistic temperature and temperature gradient conditions. The gas turbine industry routinely uses burner rig test methods which employ high velocity gas flames and internally cooled specimens. Laboratory thermal gradient rigs currently under development include an electron beam and CO_2 laser facility. These approaches have been and will continue to be valuable in the development of thermal barrier coating systems. However, the above approaches have high capital or operating costs and significant safety issues which make it difficult to site them in most laboratory facilities.

A thermal gradient rig more suitable for laboratory use is being developed (Fig. 15). The rig employs an internally cooled tubular specimen. The heat flux is generated by an inductively heated zirconia susceptor concentric with the specimen. The maximum heat flux is greater than 50 W/cm^2. The system will be capable of generating turbine relevant temperatures and temperature gradients through TBC coated superalloy specimens. The rig will feature precise control of the heat flux and forced convection internal cooling. TBC surface temperature, TBC / bond coat interface temperature, and internal surface temperatures will be measured and recorded. Provisions for introducing alternative gas environments are incorporated in the design.

Assembly of the principal elements of the system was completed in the first quarter of FY1997. The remaining components, including instrumentation, have been ordered. Start-up of the system is scheduled for the early part of FY1998.

Failure Mechanisms. The purpose of this proposed research is to identify failure mode(s), understand and evaluate failure mechanisms, and develop appropriate test methods and protocols to characterize the integrity and predict failure of thermal barrier coatings (TBCs) during thermal shock and cyclic oxidation**.** Specific tasks include the following:

1. Complete a critical review of the TBC literature to identify critical needs in thermal cyclic and mechanical/microstructural testing and evaluation. Based on this literature search, identify potentially appropriate test method(s) to predict TBC performance.

2. Obtain controlled specimens (in collaboration with Oak Ridge National Laboratory) of TBCs with various microstructures and compositions, and that have been processed by different techniques.

3. Perform mechanical/thermal cyclic tests (in collaboration with Oak Ridge National Laboratory) in simulated service environments and evaluate microstructures before and after thermal cycling.

4. Identify failure modes and evaluate failure mechanisms after thermal cyclic and mechanical testing.

5. Based on microstructural observations on failure modes, correlate the results of thermal cyclic tests with those of mechanical tests to select and develop mechanical test methodology and protocols for accurately predicting TBC performance in service environments.

Effort has continued in three areas: (1) evaluation of elastic modulus of coatings by indentation technique; (2) installation of a furnace to thermally cycle TBC specimens; and (3) conducting thermal cycling experiments on

the first TBC specimen. A brief summary of the results is presented below.

The indentation study has continued to systematically evaluate the effects of indentation load and coating orientation on the measured elastic modulus of the ZrO_2 top coat. Specifically, further results have been obtained on the elastic moduli of the ZrO_2 top coat measured as a function of indentation load on the planes parallel and transverse to the coating plane. The results are shown in Figure 16. It can be seen that the measured elastic modulus becomes insensitive to the indentation load above a critical load. This observation results from the change in indentation size relative to microstructural scale with increasing load. The indentation size increases with increasing load and hence encompasses more microstructural defects (pores, grain/lamellae boundaries, microcracks, etc.). This results in a corresponding decrease in measured elastic modulus with increasing load. However, after a critical load is reached, the extent of defect encountered by the indentation per unit area or per unit volume becomes relatively constant and the resulting elastic modulus becomes constant and insensitive to load. This constant value of elastic modulus can be used for the purpose of materials comparison/selection and design analysis.

Figure 16 also shows the effect of coating orientation on elastic modulus. A comparison of the elastic moduli measured on planes parallel (top plane) and transverse to the coating plane indicates that at lower indentation loads, elastic moduli differ very slightly and become the same at higher loads for the two orientations. These results suggest little or no anisotropy in the two orientations which is consistent with the microstructural observations.

A high temperature furnace capable of reaching 1600°C and thermal cycling TBC specimens in an oxidizing atmosphere was also installed. This furnace can be programmed to thermally cycle TBC specimens between preselected temperatures at desired time intervals. Thermal cycling experiments were initiated on air plasma-sprayed yttria partially-stabilized zirconia TBC specimens. Two specimens were subjected to a number of thermal cycles, each cycle consisting of heating the specimen to 1150°C in air, holding for 1 hour at that temperature, then cooling rapidly by fan. Specimens were taken from the furnace after a preselected number of thermal cycles and were subjected to the following testing and evaluation: (a) visual inspection to determine if the TBC had failed by spallation, (b) weight gain/loss measurement, (c) X-ray diffraction analysis of ZrO_2 top coat to characterize phase changes during thermal cycling, and (d) elastic modulus and hardness measurement by the indentation technique.

The specimen which was used for weight gain/loss study and phase evaluation was observed to fail by spallation after 92 cycles. X-ray diffraction patterns indicated little or no change in phase composition of the top surface of the ZrO_2 coat after various number of thermal cycles. Figure 17 shows weight change for TBC specimens as a function of thermal cycles. Initially, the weight gain results from the oxidation of the interface and metallic substrate, while at larger number of thermal cycles (longer exposure times) spallation of the oxide scale from the metallic substrate results in weight loss. Figure 18 shows the variation in measured elastic modulus and hardness values of the ceramic top coat with thermal cycles. Initially, the elastic modulus and hardness of the ZrO_2 top coat increases with increasing number of thermal cycles. This is believed to result from densification of the top coat. At a higher number of cycles, both elastic modulus and hardness of the top coat decrease because of an increase in microcracking. Detail edmicrostructural evaluation to characterize damage evolution during cyclic oxidation is currently in progress.

Thermophysical Properties and Thermal NDE. The primary goal of this research activity is to develop and apply state-of-the-art characterization and non-destructive evaluation (NDE) techniques to evaluate the thermal reliability, performance and stability of thermal barrier coatings (TBCs). Previous studies at ORNL and elsewhere have shown that the microstructure of both APS and EB-PVD zirconia coatings are thermally unstable

at and above 1000°C. The lamellar porosity, which exists between splats in the PS coatings, evolves into small spherical pores at high temperatures. This microstructural change results in a coating with a higher thermal conductivity since spherical pores are less effective at impeding heat flow than thin plate-like pores of equal volume. Reliable knowledge of the thermal conductivity of a thermal barrier coating is important in modeling the performance of advanced turbine systems which employ TBC systems. In addition, thermal conductivity measurements may be used to study and model the thermal stability of TBCs. As new TBC concepts are developed (e.g. multilayer, functionally graded, CVD, opacification, etc.), they require careful characterization for thermal stability and effectiveness in reducing the thermal conductivity at high temperatures.

Several techniques have been employed to study advanced thermal barrier coating systems. These techniques include xenon and laser flash thermal diffusivity, step-heat flux thermal diffusivity, 3ω thermal spectroscopy, infra-red imaging, and scanning thermal conductivity microscopy (STCM). The flash diffusivity, 3ω thermal spectroscopy, and step-heat flux systems are capable of making measurements on free standing coatings as well as coatings bonded to substrates. Flash diffusivity measurements can be made in vacuum, inert gas, oxidizing or reducing atmospheres up to 1700°C, which is significantly higher than any proposed application temperature for these materials. The 3ω technique is ideally suited for coatings that are too thin to be measured by the flash technique (thickness < 200μm). Infra-red imaging allows thermal diffusivity mapping of the surface of a coating on test coupons and components as well as the detection of subsurface damage. The scanning thermal conductivity microscope was developed to study thermal conductivity variations on a microscopic scale. This instrument will provide unique insight into the performance of functionally graded, multilayer, and partially oxidized coatings.

Thermal diffusivity and conductivity measurements are made on as-fabricated as well as thermally aged (cycled) coatings. The increases in thermal conductivity due to thermal aging are modeled as a function of temperature and time at temperature. Thermal conductivity changes can be correlated with the impurity level of the starting powders. Results from these thermal conductivity studies will be correlated with microstructural and thermomechanical investigations in order to provide a complete understanding of the factors which effect the performance and life of advanced TBCs. This understanding is a necessary step in the development of comprehensive life prediction models.

HTML's high speed IR camera has been used to demonstrate thermal NDE techniques on turbine engine blades as well as test coupons. Engine tested blades are flashed with a xenon flash lamp and the temperature decay of the surface is monitored with the ir camera. Hot regions develop over areas where the coating has delaminated from the substrate. This technique has been sucsessfully used to spot subsurface flaws between the bondcoat and substrate, cracks in substrate, thickness variations in TBCs, and the flaws between a TBC and substrate. This technique can detect flaws with a minimum lateral dimension approximately equal to its depth below the surface. New techniques are currently being developed that will improve detectability by a factor of two.

Based on guidance from the gas turbine manufacturers, decisions will be made on whether to proceed with specific characterization techniques. Consideration will also be given to conducting model verification tests in more representative gas turbine environments. This program is also being closely coordinated with related ongoing work at the HTML. This includes an HTML Industrial Fellow Program which is characterizing the thermal stability of alternate ceramic TBCs, and the HTML User Program.

Nanocrystalline powders have been prepared at Penn State University for possible applications for thermal barrier coatings. Low thermal conductivity and high temperature stability of the TBCs are very important to the gas turbine and aircraft engine industries. The purpose of the project is to develop TBCs that will not show signs of aging at engine

operating temperatures. Thermal conductivity of nanocrystalline specimens with various density, yttria content and grain size were studied.

Nanocrystalline powders made at Penn State were characterized with SEM and TEM to confirm the grain size, porosity and microstructure. Yttria contents were varied from 0% to 15%. Grain size and porosity were controlled by sintering temperature and sintering time. Thermal conductivity of the specimens was obtained using laser flash and DSC techniques. Platinum coatings were put on both sides of the specimen at Penn State to prevent laser penetration. Thermal diffusivity tests were run in nitrogen environment in two different furnaces. The maximum temperature for the tests was 1000°C. To study the aging effect some samples were tested during cooling and at room temperature after high temperature exposure.

Thermal conductivity of zirconia was found highly dependent on the yttria content. Figure 19 shows the thermal conductivity vs. temperature plots of three different yttria concentrations. The monolithic zirconia (0% yttria) showed the highest thermal conductivity and most significant temperature dependency. A power-law curve fit, AT^{-B}, was used in the plot. At 6% yttria level thermal conductivity decreased dramatically and the temperature dependency was approximated with a second-order polynomial curve fit. When the yttria content increased to 15%, thermal conductivity showed almost constant values over the entire temperature range and a simple linear relationship was used to fit the data.

Thermal aging typical for both APS and EB-PVD coatings was not observed in the Penn State specimens. Thermal conductivity stayed unchanged or decreased slightly up to 1000°C. This observation was consistent with the microstructure studies at Penn State. The effects of grain size and porosity on thermal conductivity are as yet non-conclusive. Data obtained from Oak Ridge are being analyzed at Penn State.

Westinghouse Power Generation: Westinghouse Power Generation conducted thermal diffusivity measurements on their TBCs as part of the ATS program. Air Plasma Sprayed(APS) thermal barrier coatings were prepared using several alternative ceramic materials, as possible substitutes for zirconia. The materials selected by Westinghouse all were expected to be similar to YSZ.

Eighteen specimens were tested by the laser flash diffusivity system. The specimens were free-standing coatings, about half inch in diameter and 300μm to 500μm thick. Submicron graphite coatings were applied to both sides of the specimen to make it opaque. At room temperature, the as-sprayed specimens showed very low thermal diffusivity values, ranged from 0.005 to 0.006 cm^2/s. Thermal aging at 1200°C to 1300°C for 24, 72 and 240 hours were performed at Westinghouse. Thermal diffusivity of the thermally aged specimens was found to be increased as a function of aging temperature and time.

The as-sprayed coatings and thermally aged coatings were both tested to 1200°C in argon. The effects of aging were observed on these alternative coatings. Thermal diffusivity decreased as a function of temperature up to 800°C and showed a slight increase after 800°C dependent on the previous heat treatment. Thermal diffusivity versus temperature curves of a zirconia TBC with an alternative stabilizer are shown in Figure 20. The hysterisis effect was observed in as-sprayed specimens. Thermal diffusivity increased nearly 60% after aging. The thermal aging is believed to be a result of grain growth and further densification of the ceramic coatings at elevated temperatures.

Understanding of the aging effect on thermal conductivity of TBCs is very important to the engine designers. The results provided valuable information to Westinghouse in selecting the best candidate for high performance TBCs.

Solar Turbine: Thermal conductivity testing of superalloys used by the Solar Turbine Co. were carried out at HTML. Three single crystal alloys were tested. The test specimens were machined from bars with the <001> crystal orientation parallel to the longitudinal axis of the cylinder (FCC, nickel-

base material). The materials were supplied by Cannon-Muskegon Corporation. Thermal diffusivity of the three alloys is shown in Table 4. Thermal diffusivity tests were then performed in nitrogen in a graphite furnace from 600°C to 1000°C and the results are shown in Figure 21. The diffusivity values increased as a function of temperature. Thermal transport properties of the superalloys are required for both the technology development and detailed design phases of Solar's ATS Industrial Gas Turbine Program.

Oxidation Resistance. Cyclic oxidation kinetics (1-hr cycles) at 1150°C of the single crystal alloy René N5 and Y-free derivatives with various levels of desulfurization are shown in Fig. 22. Desulfurization was performed by PCC Airfoils Inc.[9] using a proprietary in-melt technique, a post-solidification hydrogen treatment, and a combination of both. Alloy N5-A is nominally René N5 without Y and not desulfurized (5-6 ppma S); alloy N5-AH was hydrogen-desulfurized (1.3 ppma S); alloys N5-B (1.5 ppma S) and N5-C (0.8 ppma S) were melt-desulfurized; and alloy N5-BH (o.6 ppma S) was melt-desulfurized and then hydrogen annealed. Alloys N5-B and N5-C (1.5 ppma S and 0.8 ppma S, respectively) suffered weight losses due to scale spallation at earlier times than René N5 and alloys N5-AH (1.3 ppma S) and N5-BH (0.6 ppma S). Cyclic oxidation results from other work in this study indicated a consistent improvement in scale spallation behavior for alloys N5-AH, N5-BH, and N5-C, but that the order of improvement was N5-BH>N5-AH>N5-C, although chemical analysis indicated that the sulfur content of N5-C was lower than for N5-AH. Alloys N5-AH and BH had, in fact, been decarburized as a result of the hydrogen annealing part of the desulfurization process. It is possible that decarburization influenced the improvement in resistance to scale spallation by, for instance, allowing the Hf content of the alloys to play a more active role (similar Hf contents in NiAl produce slow-growing, very adherent alumina scales).

Figure 23 shows the oxidation kinetics from the same 1-hour cycle test at 1150°C for René N5, N5-A and N5-C coated (on one side) with a state-of-the-art platinum-aluminide bond coating and a top coat of yttria-stabilised zirconia (YSZ) deposited by electron beam physical vapor deposition (EB-PVD), while the other side was coated with a simple aluminide. The criterion used to assess failure of the TBCs was the loss of at least 20 percent of the ceramic layer on the flat surfaces of the specimens. The loss of small chips of ceramic from the edges of the specimens was discounted, since the specimen shape and dimensions were not optimized to accommodate a TBC. The ceramic layer on N5-A failed after 300 cycles; on N5-C failure occurred after 450-500 cycles; whereas the TBC on René N5 failed after 650 cycles. On this basis, the life of the coating on the non-desulfurized, Y-free substrate (N5-A) was approximately one half that on René N5, whereas the life of that on N5-C (≈0.8 ppma S) was approximately 75 percent that on the Y-containing alloy. The potential clearly exists for a Y-free, desulfurized alloy to achieve a similar lifetime as the Y-containing alloy.

The same EB-PVD YSZ coating was directly applied to one side of specimens of an experimental, reactive element-doped alloy (β-NiAl-Zr),[10] to demonstrate the potential spallation-free lifetime possible when the surface to which the ceramic is applied forms an 'ideal' alumina scale. Previous studies[11,12] have shown that this alloy forms an α-Al_2O_3 scale that grows almost entirely by oxygen transport, at a rate up to 2 to 4 times slower than that formed on undoped NiAl (or other undoped alumina-forming alloys), and which shows only edge spallation at temperatures in the range studied here for times in excess of 2,500 hours (oxide thickness greater than 9 μm). As shown in Fig 24, the lifetime of the ceramic layer on this substrate was more than 2,500 cycles, at least four times that of the René N5-PtAl bond coat system in the same test. Surprisingly, a YSZ coating deposited by plasma-spraying directly onto the polished surface (600 grit finish) of the b-NiAl-Zr alloy was found to spall only after 1,200 cycles, which was almost double the lifetime of the René N5-PtAl-EB-PVD YSZ system in the same test.[10]

The effectiveness of the optimally-doped β-NiAl-Zr alloy (compared to the undoped Pt-aluminide layer on the Y-doped superalloy) in

retaining an external YSZ layer in the thermal cycling tests resulted from four main factors: (1) reduced rate of growth of the oxide (2) the lack of void formation at the substrate-oxide interface (3) there were no unwanted elements able to transport to the oxidizing surface and become incorporated into the scale, and (4) there was always sufficient aluminum available for protective scale formation since there was no loss by interdiffusion with a substrate. The first two factors are manifestations of the reactive element doping in this alloy, whereas the third and fourth factors resulted from the fact that a monolithic alloy was used as the 'bond coating.' These advantages have not yet been realized in a practical coating.

FUTURE WORK

In the long-term testing effort, future work will focus on the measurement of the creep and stress rupture behavior of additional composites which are of interest to Solar Turbines and Allison Engines. Efforts to evaluate the thermomechanical behavior of TBC systems will also be initiated.

In the areas of thermophysical properties and thermal NDE, thermal diffusivity and conductivity measurements will be made on as-fabricated as well as thermally aged (cycled) coatings. The increases in thermal conductivity due to thermal aging will be modeled as a function of temperature and time at temperature. Thermal conductivity changes will also be correlated with the impurity level of the starting powders. In addition to thermal transport and NDE studies, this task will also investigate the relative thermal expansion of TBCs as a function of temperature, time, and oxidation. These measurements will be made using a custom designed bi-layer dilatometer. Measurements can be made in vacuum, inert gas, or oxidizing atmospheres up to 1650° C.

Results from these thermal conductivity studies will be correlated with microstructural and thermomechanical investigations in order to provide a complete understanding of the factors which effect the performance and life of advanced TBCs. This understanding is a necessary step in the development of comprehensive life prediction models.

In the Residual Stress area, future effort will be placed upon the measurement of strains in TBC systems at elevated temperatures. This will also include the measurement of strains and crystallographic texture in the oxide scale. Finally, the strains as determined from x-ray diffraction will be compared to at least two techniques (Raman spectroscopy , microfluorescence, bilayer dilatometry, and neutron diffraction).

Based on guidance from the gas turbine manufacturers, decisions will be made on whether to proceed with specific characterization techniques. Consideration will also be given to conducting model verification tests in more representative gas turbine environments. This program is also being closely coordinated with related ongoing work at the High Temperature Materials Laboratory (HTML). This includes an HTML Industrial Fellow Program which is characterizing the thermal stability of EB-PVD TBCs, and the HTML User Program

REFERENCES

(1) E. E. Hoffman, M. A. Karnitz, J. H. DeVan, R. S. Holcomb, D. Anson, and R. W. Harrison, R. P. Allen, "Materials/ Manufacturing Plan for Advanced Turbine Systems Program," April 1994, DOE-OR-2007.

(2) M. van Roode, "Ceramic Retrofit Program," pp. 77-93 in Proceedings of the Joint Contractors Meeting: FE/EE Advanced Turbine Systems Conference FE Fuel Cells and Coal-Fired Heat Engines Conference, DOE/METC-93/6132, August 1993.

(3) M. van Roode, "Ceramic Stationary Gas Turbine Development Program-Third Annual Summary," to be published in the proceedings of ASME Turbo Expo '96 Conference, Birmingham, UK, June 10-13, 1996.

(4) R. Wenglarz, S. Ali, and A. Layne, "Ceramics for ATS Industrial Turbines," to be published in the proceedings of ASME Turbo Expo '96 Conference, Birmingham, UK, June 10-13, 1996.

(5) A. A. Wereszczak, M. K. Ferber, T. P. Kirkland, M. R. Foley, and R. L. Yeckley, "Evolution of Stress Failure Resulting from Stress/Oxidation Damage in a Hot Isostatically Pressed Silicon Nitride at Elevated Temperatures," *J. Amer. Ceram. Soc.*, **78** [8] 2129-40, 1995.

(6) A. A. Wereszczak, M. K. Ferber, T. P. Kirkland, and K. L More, “Evolution of Oxidation and Creep Damage Mechanisms in HIPed Silicon Nitride Materials," pp. 457-66 in Plastic Deformation of Ceramics, edited by R. C. Bradt, Plenum Press, New York, 1995.

(7) E. Lara-Curzio and M. K. Ferber, "Stress-Rupture of Continuous Fiber Ceramic Composites at Intermediate Temperatures, " submitted. J. Mater. Sci., (1996).

(8) C. Sarioglu, J. R. Blachere, F. S. Petit and G. H. Meier, “Room Temperature and “In-Situ” High Temperature Strain or Stress Measurements by XRD Techniques,” University of Pittsburgh, preprint.

(9) C. S. Kortovich, R. M. Garlock, and C. R. Hayes: “Turbine Airfoil Manufacturing Technology,” Paper No. 97-GT-428, presented at the 42nd ASME Gas Turbine and Aeroengine Congress, Exposition, and Users Forum, Orlando, Florida, June 1997.

(10) B. A. Pint, I. G. Wright, W. Y. Lee, Y. Zhang, K. Prüßner and K. B. Alexander: “Substrate and bond coat compositions: factors affecting alumina scale adhesion,” Mat. Sci. and Eng., 1998, in press.

(11) B. A. Pint, J. R. Martin and L. W. Hobbs: “^{18}O/SIMS characterization of the growth mechanism of doped and undoped α - Al_2O_3,” Oxid. Met., 1993, **39**, 167-95.

(12) B. A. Pint: “The oxidation behavior of oxide-dispersed b-NiAl: I. Short-term performance at 1200°C,” Oxid. Met., 1998, in press.

ACKNOWLEDGMENT

The technical and program guidance of DOE Energy Efficiency and Renewable Energy Program Managers Patricia Hoffman and DOE Morgantown Energy Technology Technical Manager, Chuck Alsup. We are also grateful for the guidance of our gas turbine industry partners.

Table 1. Summary of Tensile and Flexure Specimen Matrix Examined in this Program

Material	Supplier	No. of Tensile Specimens	No. of Flexure Specimens
SA SiC	Carborundum Company Niagara Falls, NY 14302-0832	50	205
SN88 Si_3N_4	NGK Insulators, LTD Nagoya, Japan	50	205
NT164 Si_3N_4	Saint-Gobain/Norton Industrial Ceramics Northboro, MA 01532-1545	126	205
AS800 Si_3N_4	AlliedSignal Ceramic Components	33	0
SiC/DIMOX	Dupont-Lanxide	10	0

Table 2. Summary of Test Protocol for Each Material System

Material	Test Type	Temperatures (°C)
SA SiC	-Flexural Dynamic Fatigue	1350
	-Tensile Creep	1150
	-Tensile Stress Rupture	1038
SN88 Si_3N_4	-Flexural Dynamic Fatigue	1350
	-Tensile Creep	1150
	-Tensile Stress Rupture	1038
NT164 Si_3N_4	-Flexural Dynamic Fatigue	1350
	-Combined Dynamic and Interrupted Stress Rupture	1150
		1038
AS800 Si_3N_4	-Tensile Creep	1350
	-Tensile Stress Rupture	1316
		1100
		990
SiC/DIMOX	-Tensile Creep	1000
	-Tensile Stress Rupture	1100
	-Stress Relaxation	1200

Table 3 . Phases Present In The Top Surface Of The Bond Coat Before And After Heat Treatment.

Condition	Phase	Lattice parameters (Å) a (Å)	c (Å)	ICDD Card #
As-received	AlNi	2.90		44-1108
Heat Treated	AlNi	2.90		44-1108
Heat Treated	$AlNi_3$	3.59		09-0097
Heat Treated	Al_2O_3	4.77	12.94	10-0173
Heat Treated	trace oxide phase			

Table 4. Room Temperature Thermal Diffusivities of the Three Super Alloys

Sample	Diffusivity (cm^2/s)
CMSX-4 (No. 1)	0.0226
CMSX-4 (No. 2)	0.0227
CMSX-10 (No. 1)	0.0228
CMSX-10 (No. 2)	0.0236
CMSX-11 (No. 1)	0.0268
CMSX-11 (No. 2)	0.0261

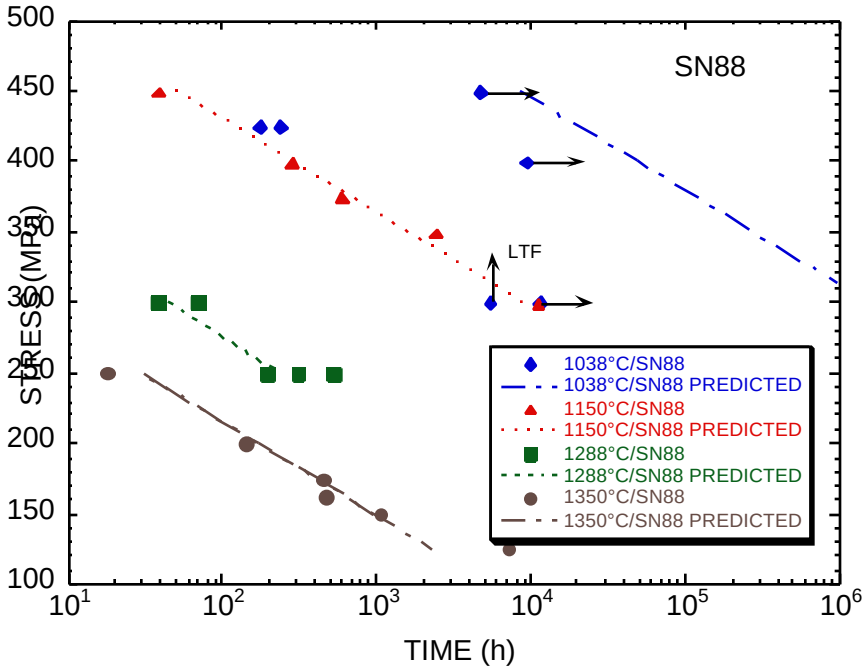

Figure 1. Stress Rupture Data Obtained for the SN88 Silicon Nitride

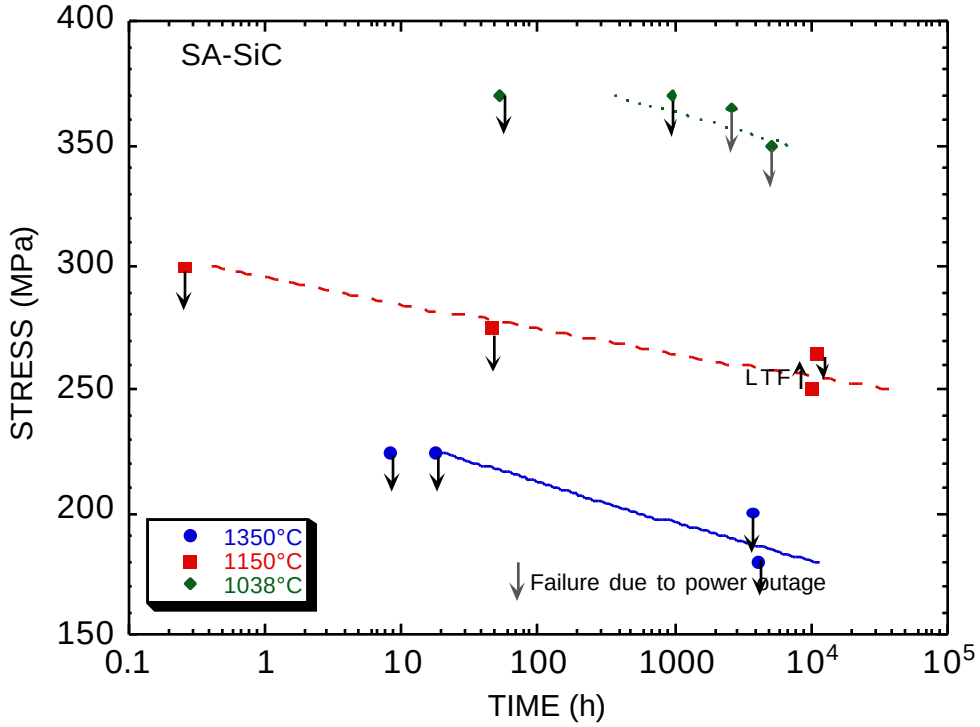

Figure 2. Stress Rupture Data Obtained for the SA SiC Silicon Carbide (Note that LTF indicates that the specimen was loaded to failure)

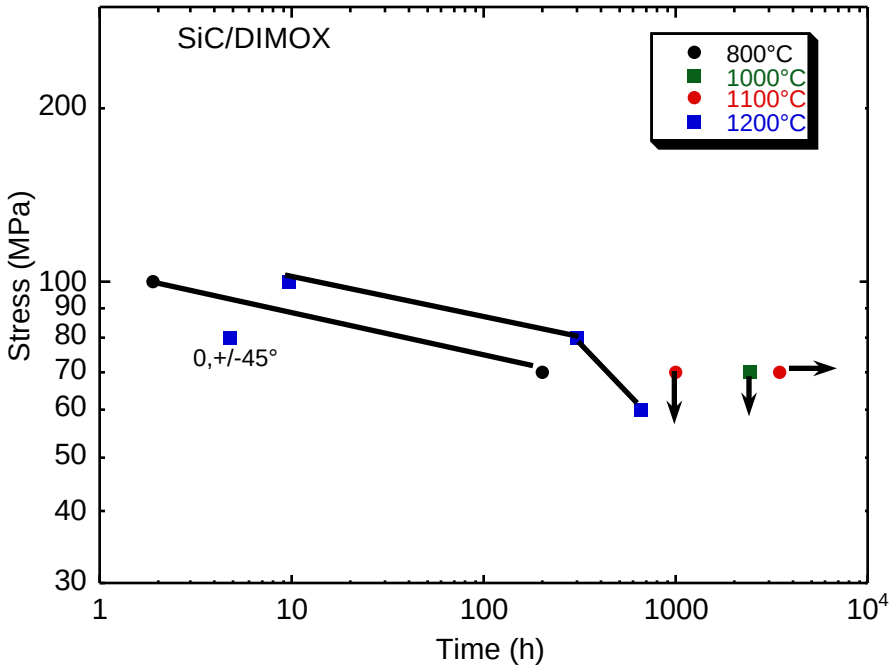

Figure 3. Stress Rupture Data Obtained for the SiC/DIMOX Composite

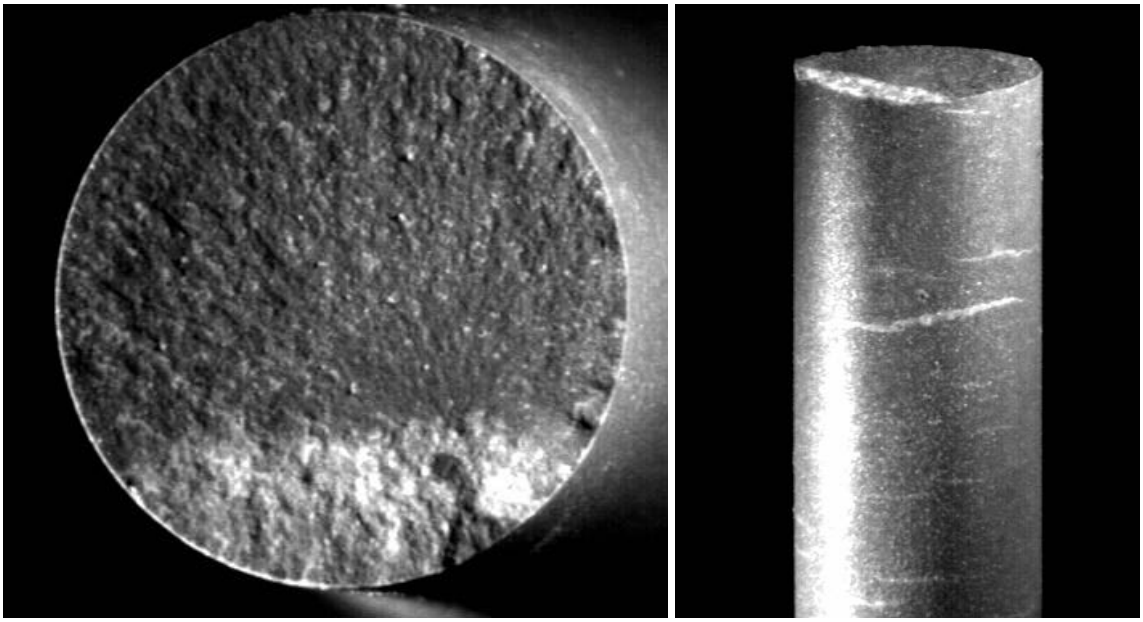

Figure 4. Fracture Characteristics of SN88 Specimen Tested At 1350°C and 125 Mpa

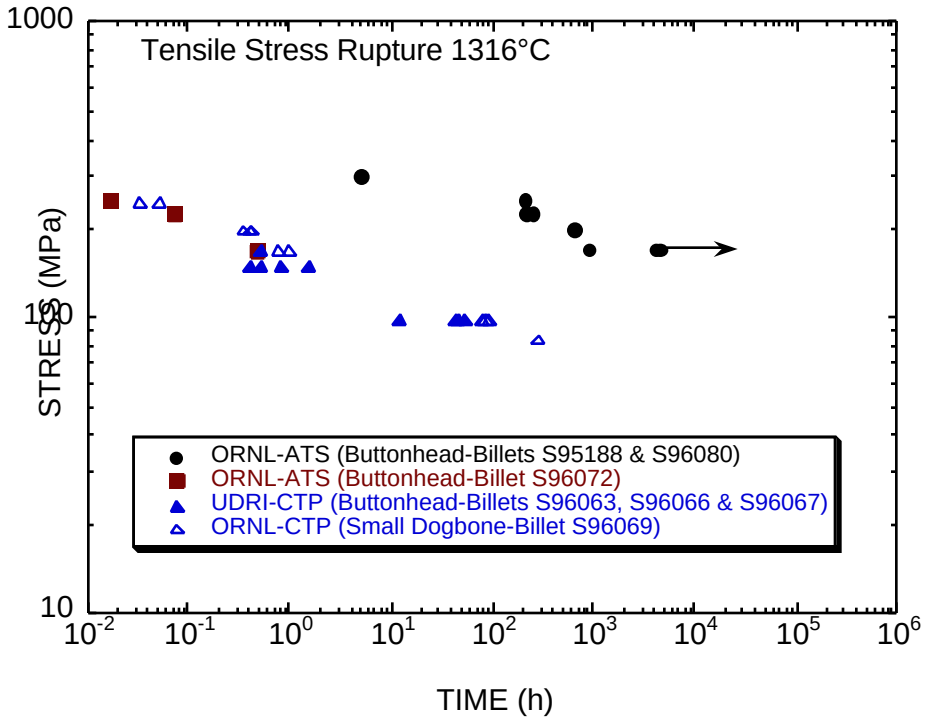

Figure 5. Stress Rupture Data Generated for the AS800 Silicon Nitride Tested At 1316°C

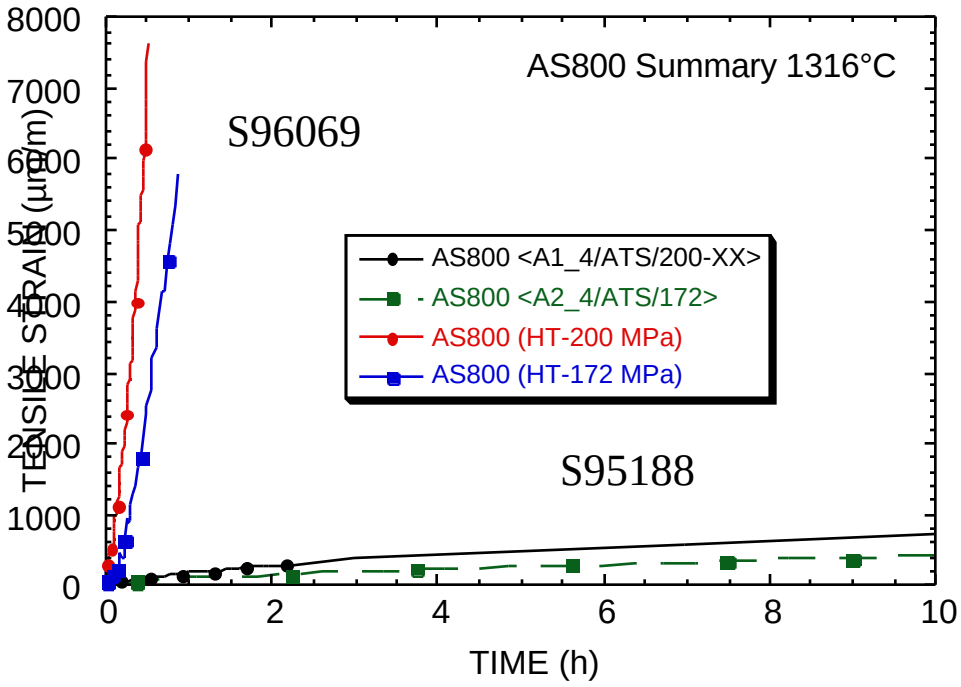

Figure 6. Comparison of Creep Deformation Behavior of AS800 Tensile Specimens Fabricated from two Different Billets.

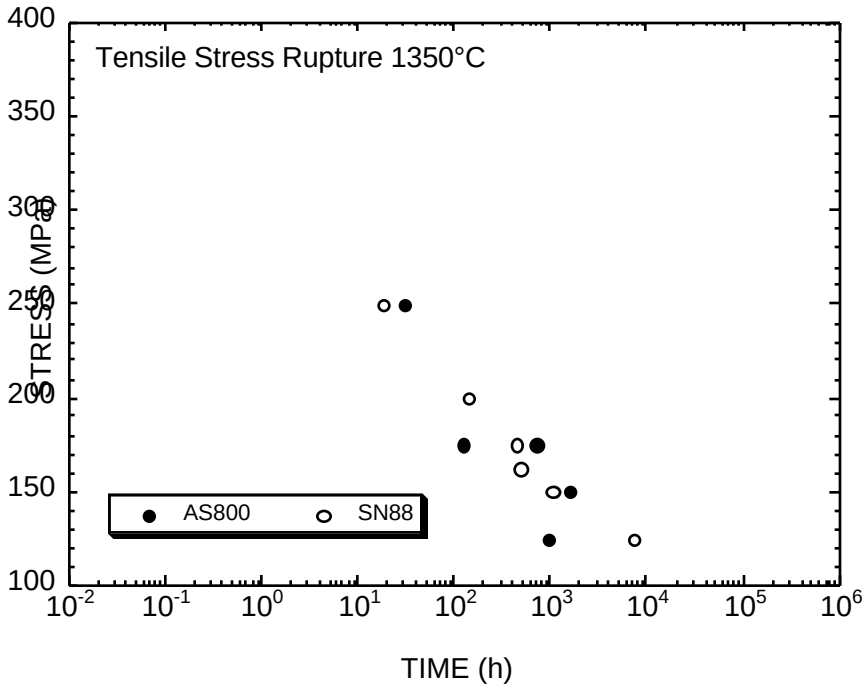

Figure 7. Comparison of the Stress Rupture Data Obtained for AS800 and SN88 at 1350°C

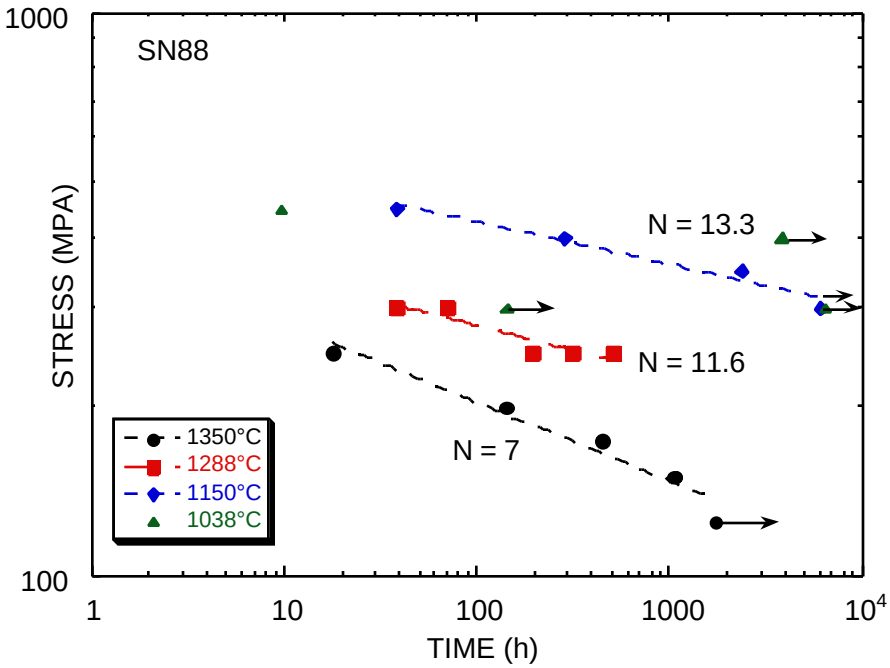

Figure 8. Effect of Temperature Upon the Stress Rupture Power-Law Exponent, N, for SN88 Silicon Nitride

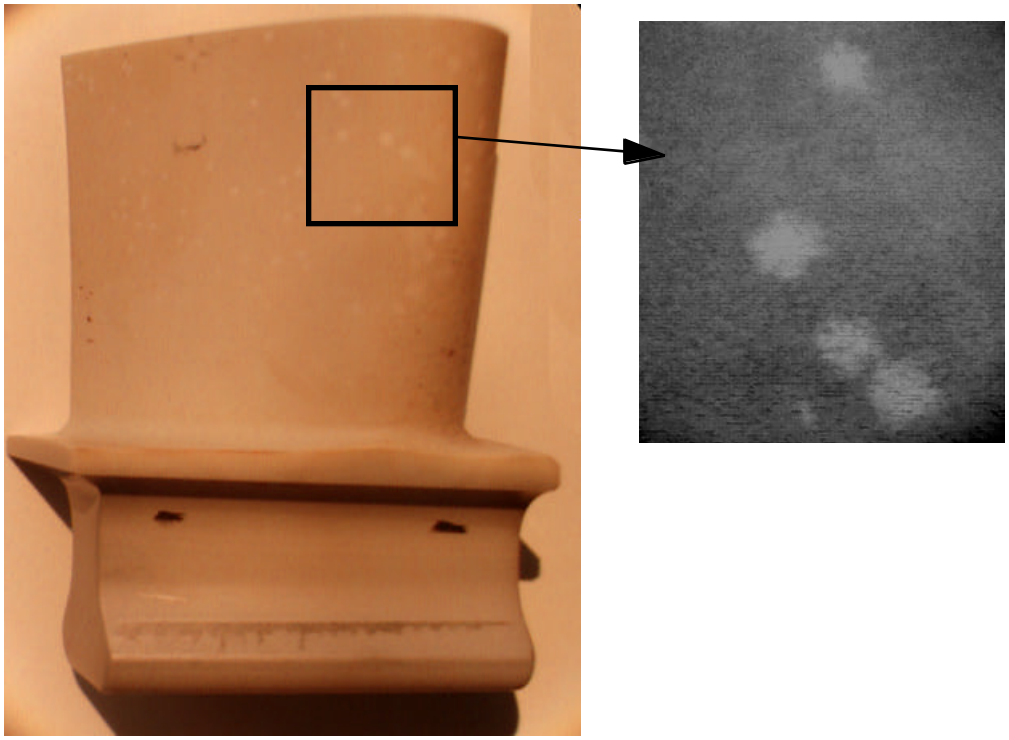

Figure 9. Macroscopic View of Post-Test Blade (AS800 S96096 03)

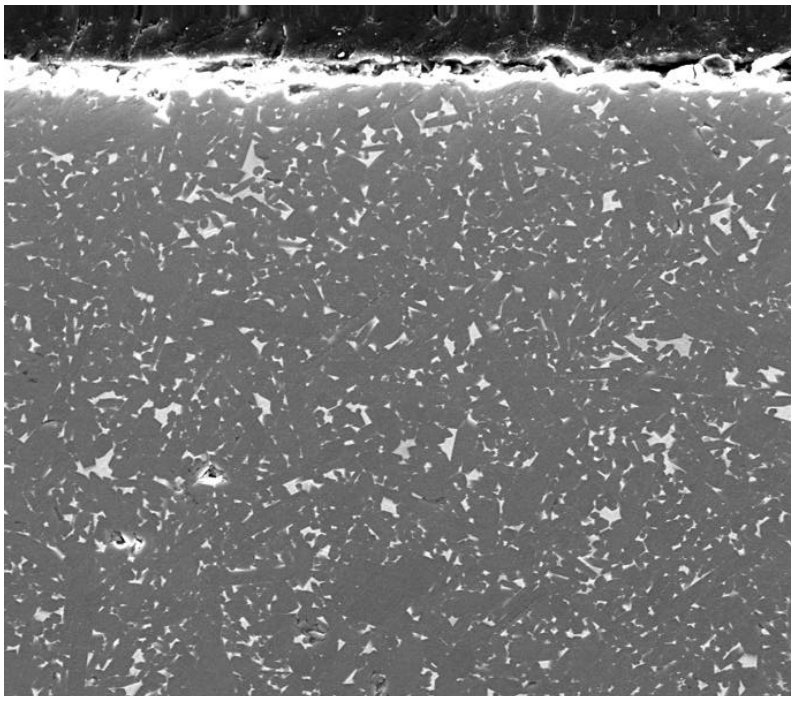

Figure 10. Cross Section (2000X) of As-Received Blade (AS800 S96058)

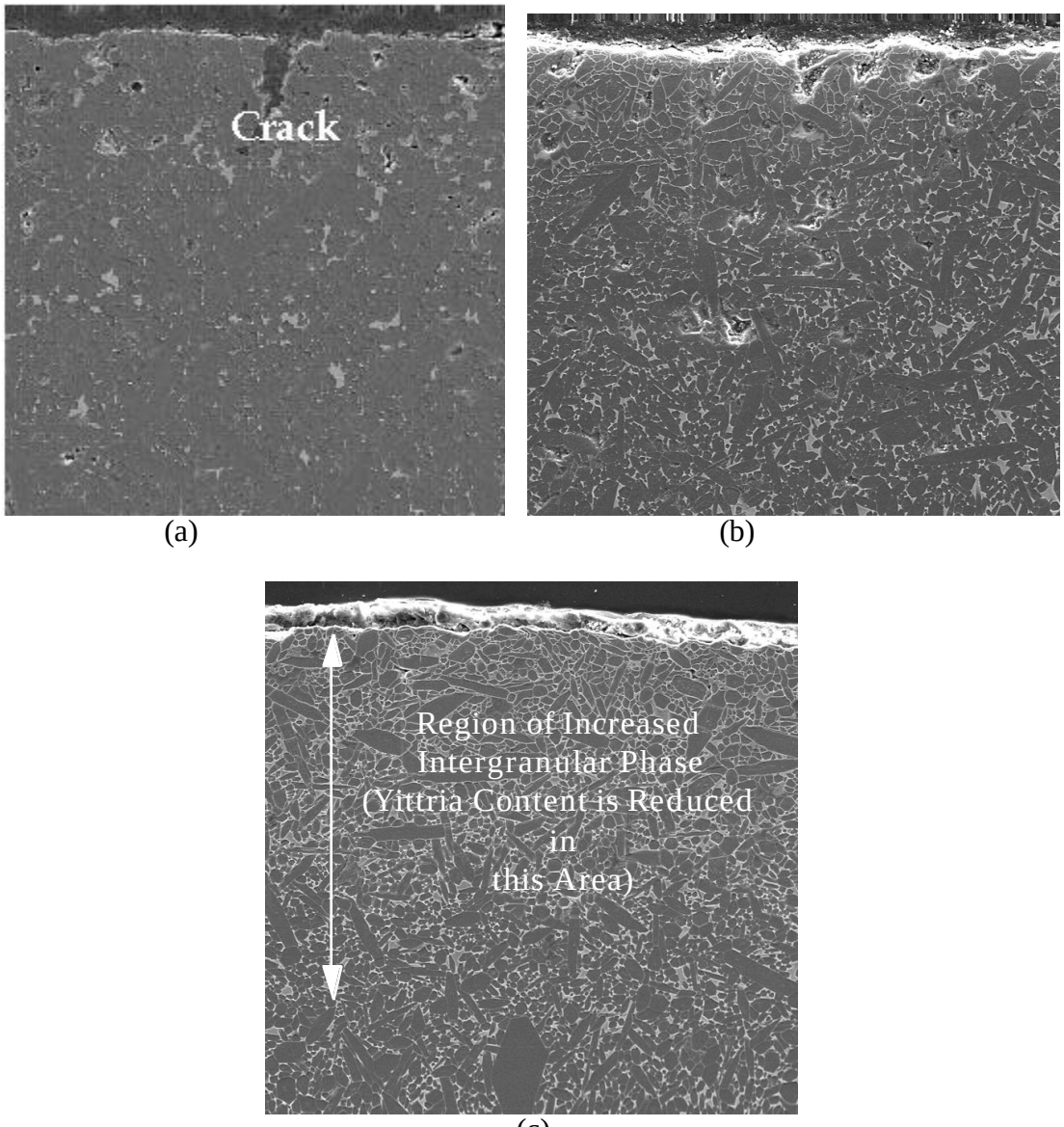

(a) (b)

(c)

Figure 11. Cross Sections (2000X) of Post-Test Blades: (a) AS800 S96062 08, (b) AS800 S96096 03, and (c) AS800 S96065 05

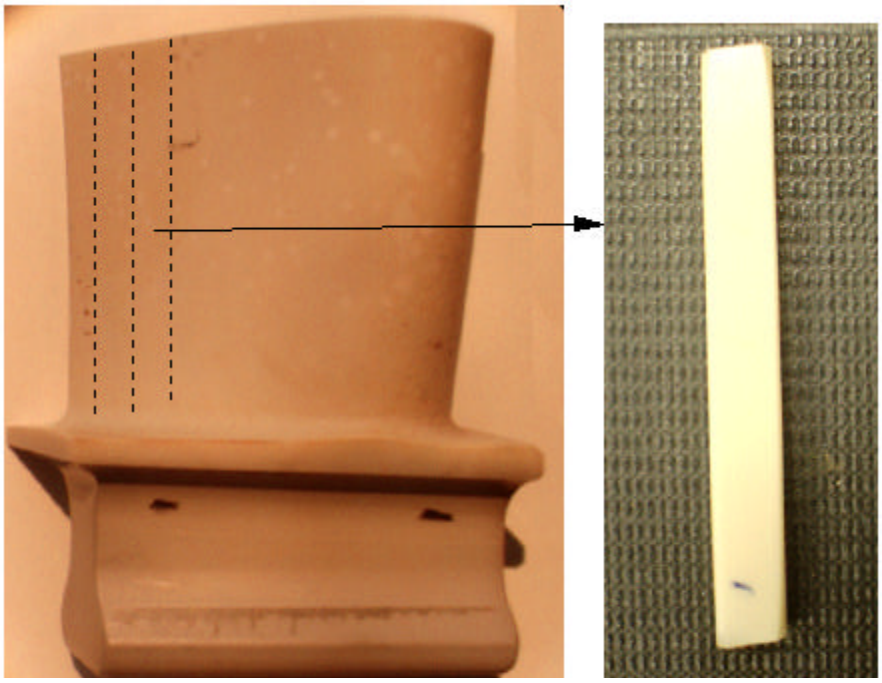

Figure 12. Sectioning of Post-Test Blade, AS800 S96096-03, into Flexure Specimens

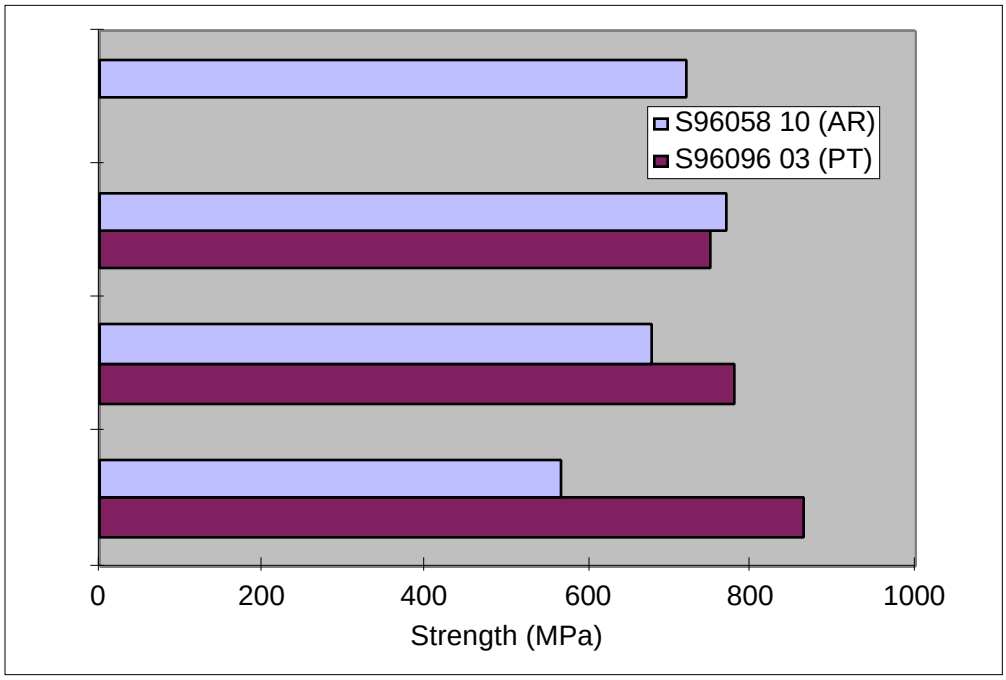

Figure 13. Strength of As-Fabricated (AR) and Post-Test (PT) (100 h) Blades

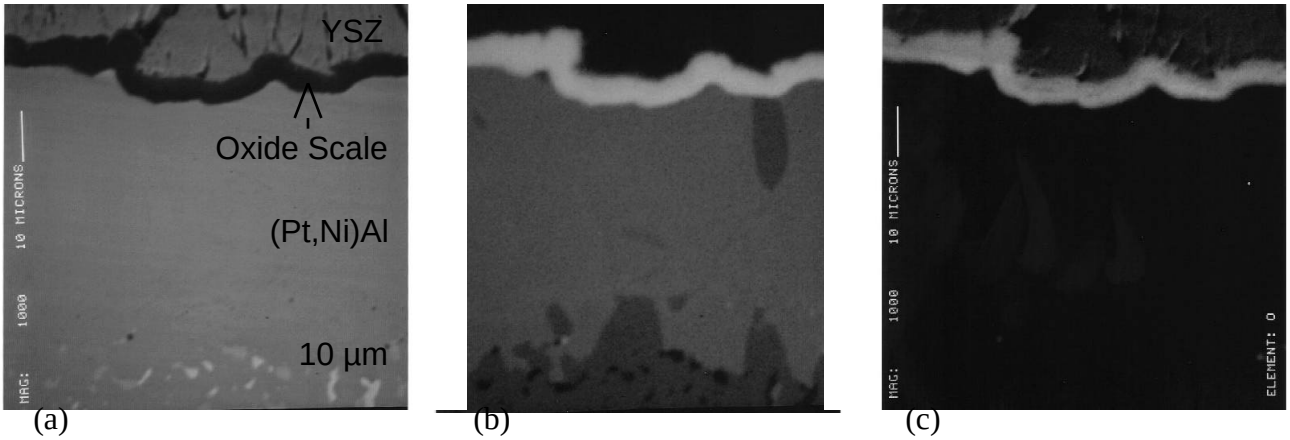

Figure 14. Micrographs from an AElectron Microprobe Showing the regions of Aluminum (b) and Oxygen (c) Concentrations Relative to the Backscattered Electron Image (a) of a Polished Cross-Section of the Heat Treated Specimen. In (b) and (c), Regions of Light/White Contrast Indicate High Concentrations of the Element Relative to the Micrograph.

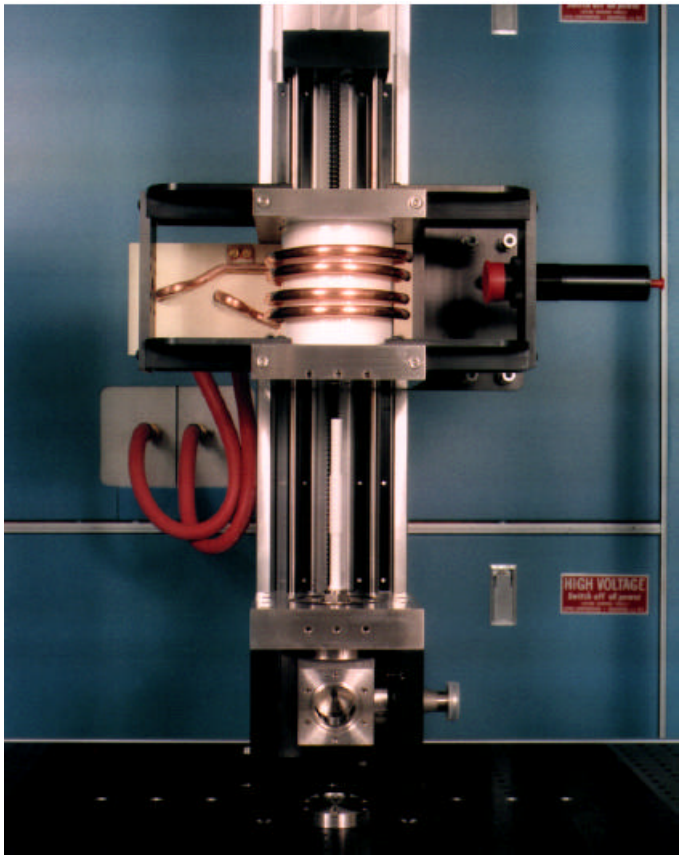

Figure 15. Thermal Gradient Test Facility

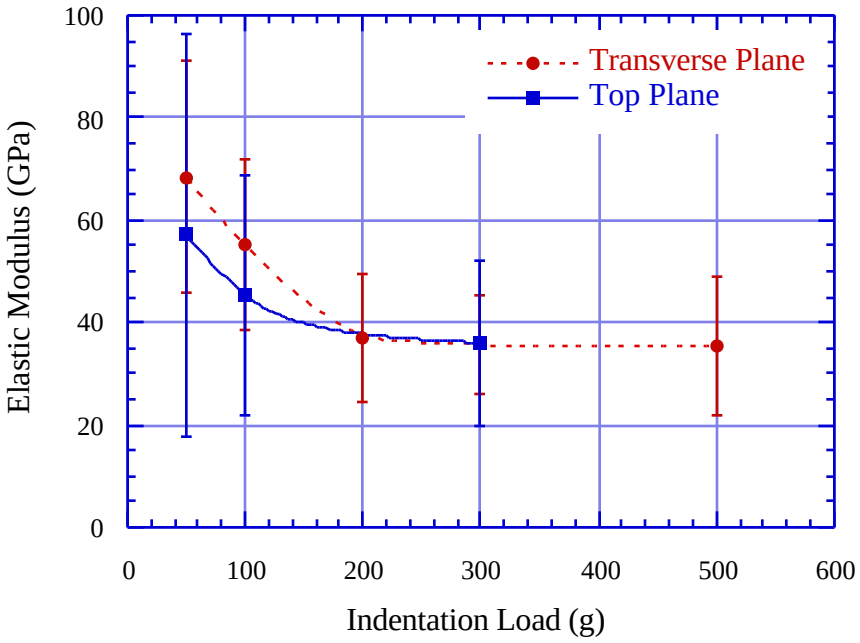

Figure 16. Dependence of Elastic Modulus on Indentation Load for Indentations Made on the Planes Parallel and Normal to the Coating Plane

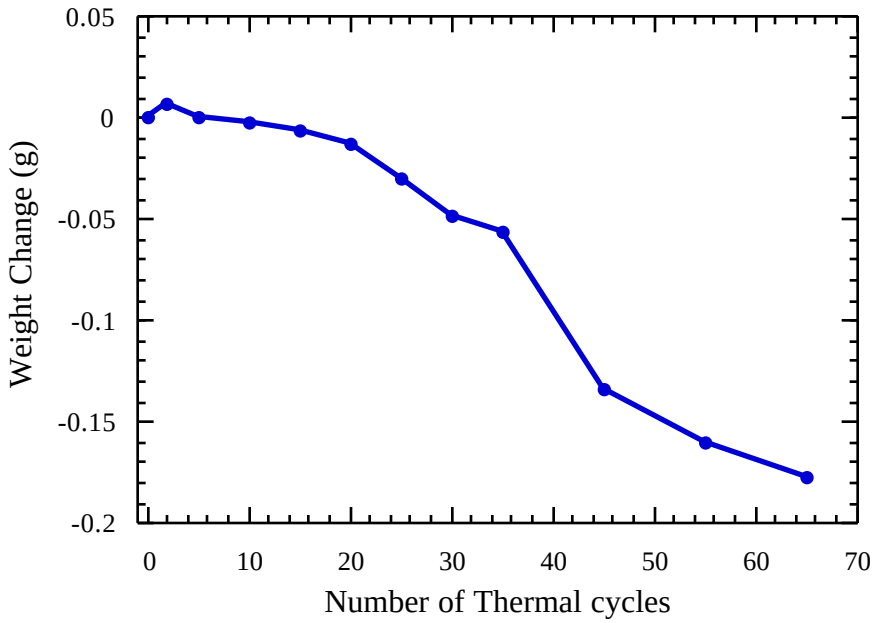

Figure 17. Weight Gain/Loss of TBC Specimen as a Function of Thermal Cycles

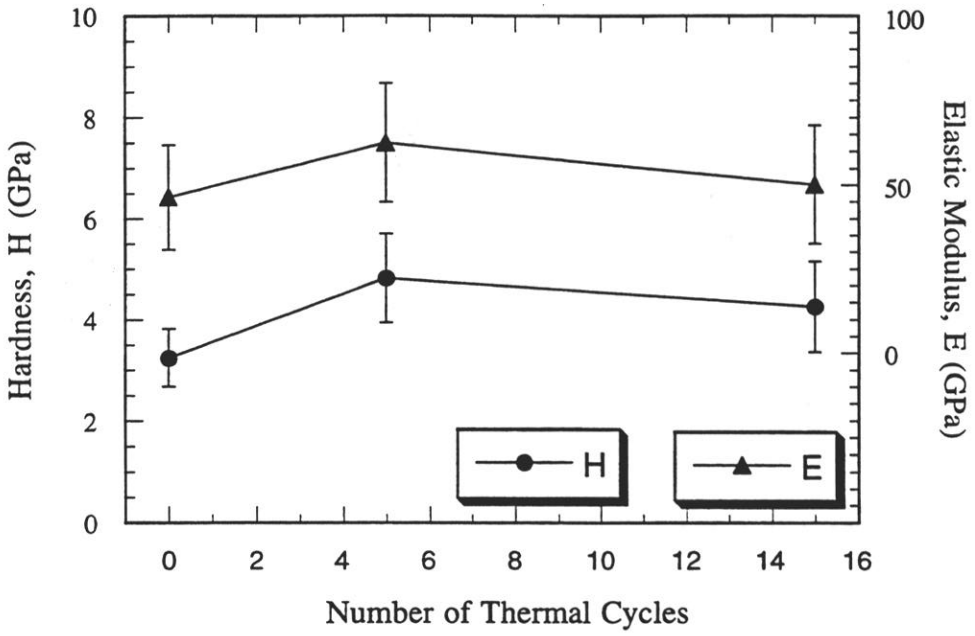

Figure 18. Hardness(H) and Elastic Modulus(E) of ZrO_2 Top Coat as a Function of Thermal Cycles

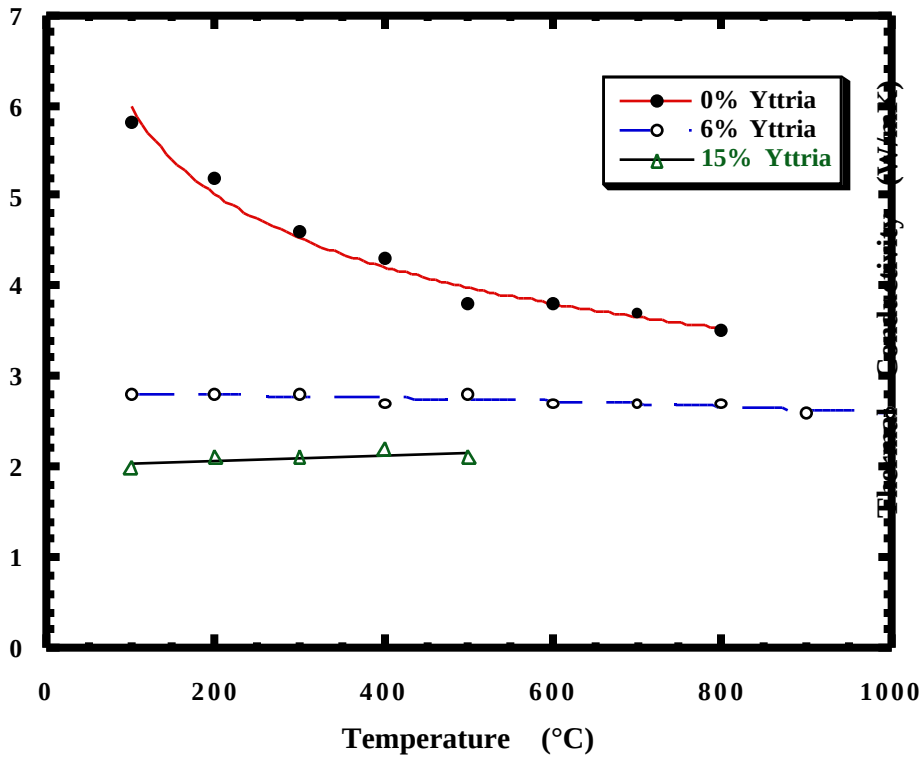

Figure 19. Thermal Conductivity of Three Specimens with Different Yttria Contents

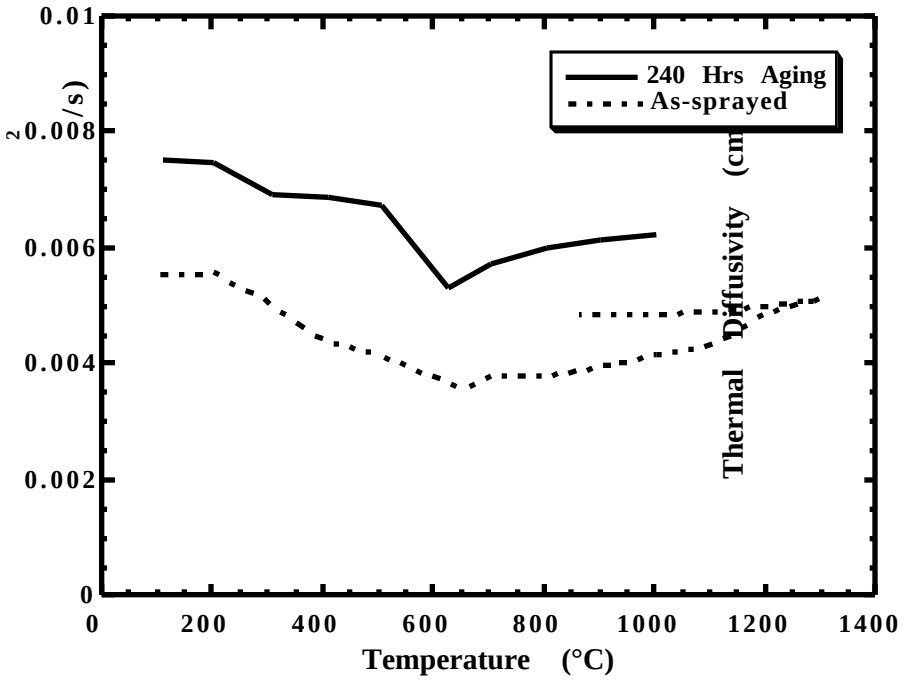

Figure 20. Thermal Diffusivity of a Zirconia TBC with an Alternative Stabilizer Before and After Thermal Aging

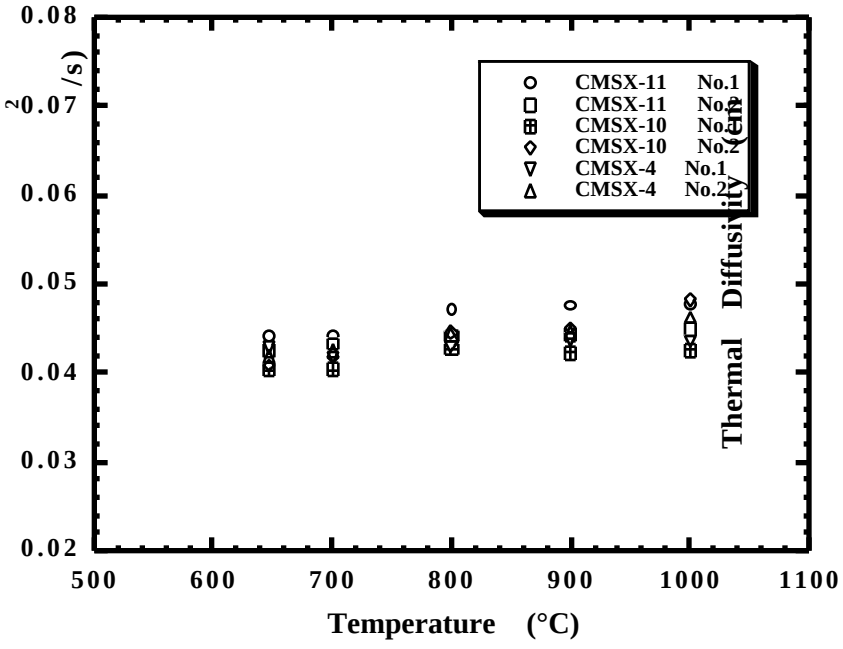

Figure 21. Thermal Diffusivity as a Function of Temperature

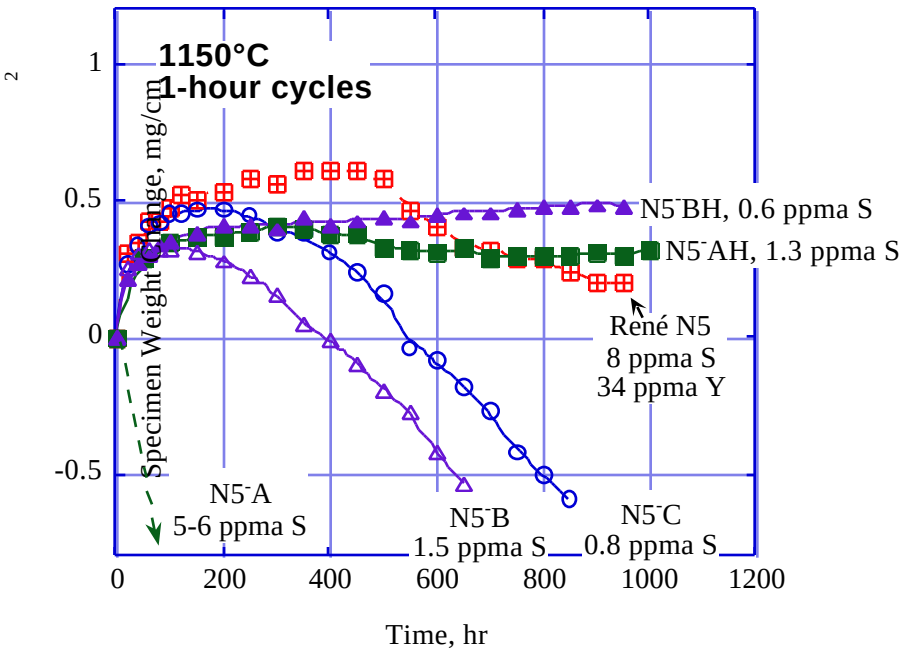

Figure 22. Cyclic Oxidation Kinetics of Single Crystal Alloy René N5, Y-free, and Y-free and Desulfurized Derivatives

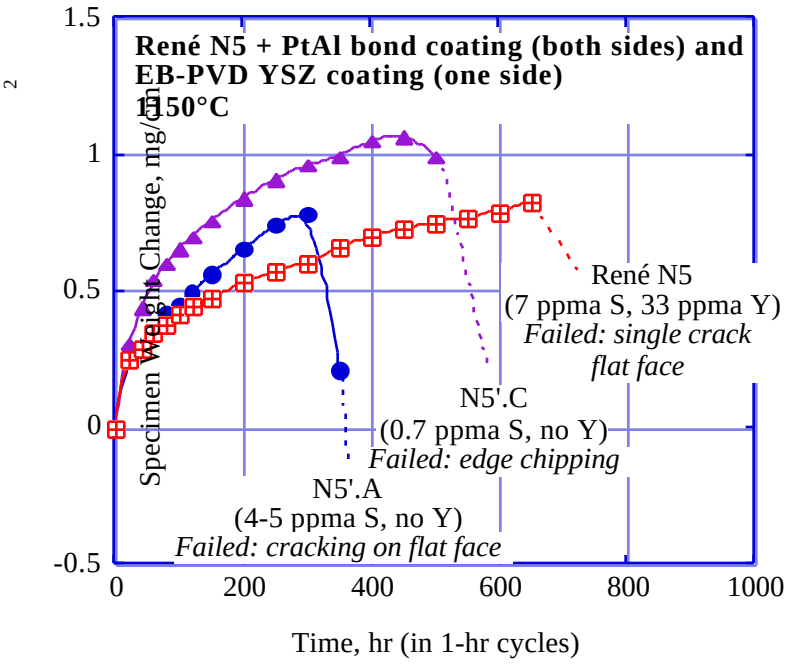

Figure 23. Cyclic Oxidation Kinetics (1-hr cycles, 1150°C) of René N5 and Y-free Plus Desulfurized Variant Substrates with State-of -the -Art TBCs

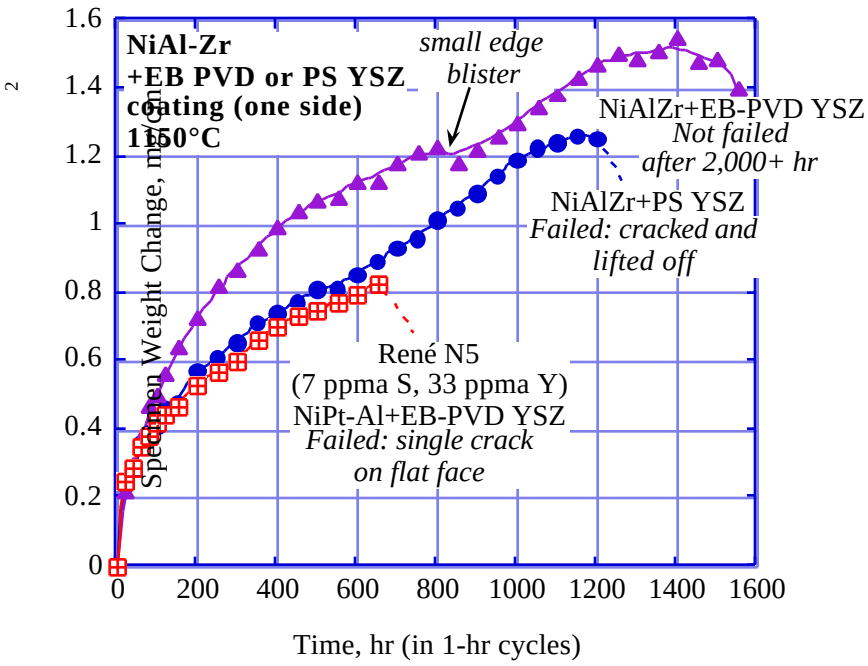

Figure 24. Comparison of Cyclic Oxidation Kinetics (1-hr cycles, 1150°C) of René N5 and β-NiAl-Zr Substrates with State-of-the-Art TBCs